ISSN 2176-5480

22nd International Congress of Mechanical Engineering (COBEM 2013)
November 3-7, 2013, Ribeirão Preto, SP, Brazil

INFLUENCE OF REPAIR WELDING CYCLES ON THE CORROSION RESISTANCE OF 2304 DUPLEX STAINLESS STEEL

Renato Altobelli Antunes
Universidade Federal do ABC (UFABC), Centro de Engenharia, Modelagem e Ciências Sociais Aplicadas (CECS), R. Santa Adélia 166, CEP: 09210-170, Santo André - SP
Camilo Augusto Fernandes Salvador
Universidade Estadual de Campinas (UNICAMP), Cidade Universitária "Zeferino Vaz", Distro de Barão Geraldo, CEP: 13083-970, Campinas – SP
e-mails: csalvador@fem.unicamp.br; renato.antunes@ufabc.edu.br

Abstract. *Flux-cored arc welding (FCAW) is an automatic welding process widely employed to join duplex stainless steel structures in industrial plants because of its high productivity. However, when multiple passes are performed, this process can lead to the formation of non-metallic inclusions originated from the slag in the fusion zone. In this case, the welded joint can be repaired using the same welding process. Some regions next to the heat affected zone are not removed during the repairing operation. Thus, these regions are subjected to repeated welding cycles and to a high heat input which can cause microstructural alteration that impair the corrosion resistance of the welded material. The aim of this work was to study the corrosion resistance of 2304 duplex stainless steel plates joined using the FCAW process and repaired using the same process. The influence of the repair procedure on the corrosion resistance of the welded joints was evaluated using potentiodynamic polarization and chronoamperometric curves which allow the determination of the critical pitting temperature of the samples. The microstructure obtained after each repair cycle was evaluated using optical microscopy and scanning electron microscopy. The results showed that the corrosion resistance was depressed as the number of repair cycles increased.*

Keywords: *2304 duplex stainless steel, repair welding cycle, FCAW, critical pitting temperature*

1. INTRODUCTION

The current annual production of duplex stainless steels (DSS) reaches around 2.10^5 t, representing less than 1% of the total amount of stainless steels produced worldwide, even though, it has increased 100% in the last decade (Charles, 2008). In 2005, the DSS became the dominant material in paper and pulp facilities for manufacturing paper digesters, replacing the austenitic stainless steels traditionally employed for this application. The DSS allowed for thinner plates to be used and presented diminished corrosion rates in comparison with AISI 316 stainless steel equipment. Arc welding processes such as gas metal arc welding (GMAW) and flux cored arc welding (FCAW) are widely used in the manufacturing of DSS-based pressure vessels (Tuomi, 2000). The FCAW process generates a slag due to the presence of the flux. As a result, gaseous species released during flux melting generate a protective atmosphere, eliminating the need for a protection gas to be used. The process is automatized which is an attractive feature for practical engineering applications (Marques, 2009). However, the weld bead needs to be cleaned at each welding pass to remove the slag, thus reducing the process productivity. If the cleaning procedure is not properly carried out, then non-metallic inclusions will contaminate the weld bead. In this case, it has to be partially removed and repaired. According to Tuomi (2000), approximately 2% of the welding procedures of DSS are reproved and need to be repaired. Some regions of the heat-affected zone (HAZ) are not removed to execute the repair cycle. Hence, the repaired zones suffer repeated thermal cycles and this can markedly affect the corrosion behavior of the welded joint (Tan et al., 2012).

Welding cycles are likely to produce microstructural transformations of DSS in the HAZ and fusion zone (FZ), leading to an unbalanced fraction of the austenite and ferrite phases. In this respect, the corrosion resistance of welded joints can be seriously affected, especially the pitting corrosion behavior of the welded DSS (Ogawa and Koseki, 1989). In the same way, the precipitation of undesirable phases such as chromium nitrides and carbides in the HAZ or FZ can deteriorate the corrosion properties too (Tan et al., 2011). The thermal history of the welded plate has a direct influence on its corrosion behavior (Zhang et al., 2012).

In spite of the well-known influence of welding cycles on the corrosion behavior of DSS, investigations focused on the effects of repair welding cycles on the corrosion resistance of these materials are not found in the literature. In this context, the aim of the present work was to study the effect of three different repair welding cycles on the corrosion resistance of the 2304 (UNS S32304) duplex stainless steel. FCAW was chosen as the welding procedure. The corrosion resistance was evaluated by potentiodynamic polarization curves and by determining the critical pitting temperature (CPT). Microstructural alterations were observed by optical microscopy and scanning electron microscopy (SEM) to give support to the observed corrosion properties of the welded joints.

ISSN 2176-5480

2. EXPERIMENTAL

2.1 Material and welding procedure

The base metal used in this work was a commercial DSS 2304 (UNS S32304) sheet of 10 mm thick. The sheet was provided by Arcellor Mittal in the form of hot rolled and annealed sheet and its chemical composition is shown in Tab. 1. Four retangular pieces with dimensions of 200 mm x 100 mm were chamfered in a universal milling machine (Fig. 1) and welded (in pairs) using the FCAW process for both the root and filling passes. Butt weld was carried out in the flat position 1G with partial penetration which demanded repair of the root in the backside of the welded joint.

Table 1. Chemical composition of the DSS 2304 sheet used in this work (wt.%).

C (%)	Cr	Cu	Mn	Mo	N	Ni	P	S	Si
0.018	22.550	0.424	1.350	0.259	0.001	3.570	0.025	0.001	0.360

Figure 1. Scheme of the welded specimens.

The filler metal was a DSS 2209 (UNS S32209; chemical composition shown in Tab. 2) in the form of a tubular wire of 1.20 mm diameter (Kestra, model KST TUB 4462 GFP), according to the AWS A5.22-95 (R05). The dimensions of the welded specimens are indicated in Fig. 2. The weld root was backed using a ceramic tile (Gullco, model 1G43R). The protection gas was a 75%Ar-35%CO_2 mixture at a flow of 16-19 $L.min^{-1}$. Additionally, in the root pass 99.9%Ar was used in the backside of the joint at a flow of 20 $L.min^{-1}$. The welding parameters were: reverse polarity, potential 23-25V, current 125-175 A, speed 2.2–4 $mm.s^{-1}$ and maximum heat input 1.32 $kJ.mm^{-1}$. Temperature between passes was kept below 150 ºC and controlled by means of a digital thermometer coupled to a type-K contact thermocouple.

Table 2. Chemical composition of the DSS 2209 tubular wire used in this work (wt.%).

C (%)	Cr	Cu	Mn	Mo	N	Ni	P	S	Si
0.028	22.540	0.343	1.370	3.040	0.080	10.000	0030	0.003	0.540

The welded sheet was divided in three specimens of 60 mm. The first and last 10 mm of the weld bead were separated and disposed. One piece was not repaired. One piece was repaired once and one piece was repaired twice. The repair cycles were carried out in the same face. Each repair cycle consisted of two passes (passes 5 and 6 in Fig. 2). The specimens are designated as R0, R1 and R2, where the algarism indicates the number of repair cycles carried out for each specimen. Three different specimens of each condition were used for the electrochemical measurements.

2.2 Electrochemical measurements

The specimens for the electrochemical measurements were prepared according to the following set of operations: i) a total transversal section of the weld joint comprising the HAZ, FZ and the base metal was cut from the welded sheet; ii) a copper wire was adhered to the specimen using conductive silver coloidal paste; iii) the specimen was embedded in

ISSN 2176-5480

cold-setting resin; iv) after complete curing, the specimen was mechanically ground using silicon carbide paper in the following sequence #180, #400, #600 and #1200; the surface finishing was carried out by polishing the specimens with a 6 m diamond paste.

Potentiodynamic polarization curves and chronoamperometric curves were acquired using Autolab PGSTAT100 potentiostat/galvanostat. A conventional three-electrode arrangement was used for the measurements with a platinum wire as the counterelectrode, a standard calomel electrde (SCE) as reference and the welded specimens as the working electrodes. For the potentiodynamic curves the potential range was from -0.3 V_{SCE} below the open circuit potential up to 1.0 V_{SCE} at a scanning rate of 0.001 $V.s^{-1}$.The electrolyte was a 3.5wt.% NaCl solution at room temperature.

The chronoamperometric curves were used to determine the critical pitting temperature (CPT) of the specimens. In this case the electrolyte was a 1 M NaCl solution. The experimental procedure comprised an initial cathodic polarization step at -0.9 V_{SCE} for 180 s. Next, the open circuit potential was monitored during 600 s. After this stabilization period, the chronoamperometric curve was obtained at a constant voltage of 0.25 V_{SCE}. The testing cell was initially put in an ice bath. The temperature was monitored using a type-K thermocouple coupled to a digital thermometer. When the temperature reached 12 ºC the cell was removed from the ice bath and put in a thermostatic bath at 45 ºC. The electrical current was monitored by the potentiostat after the cell was put in the thermostatic bath. The heating rate of the electrolyte was determined as 3.5 $ºC.min^{-1}$ up to 25 ºC and 1.5 $ºC.min^{-1}$ for higher temperatures. Based on literature reports (Tan et al., 2012), the CPT was determined as the temperature corresponding to a current density of 100 $m.cm^{-2}$.

2.3 Microstructural characterization

Quantification of the relative fractions of austenite and ferrite phases was carried out by optical microscopy (microscope Olympus BX60M). The specimens were electrolytically etched in a 30 wt.% KOH solution at 3 V for 45 s. Another electrolytic attack was performed to reveal the presence of possible deleterious phases such as chromium carbides or nitrides using a 10 wt.% oxalic acid solution (7 V for 30 s). Scanning electron microscopy (SEM) was also performed to perform this analysis (microscope Jeol, JXA 840-A)

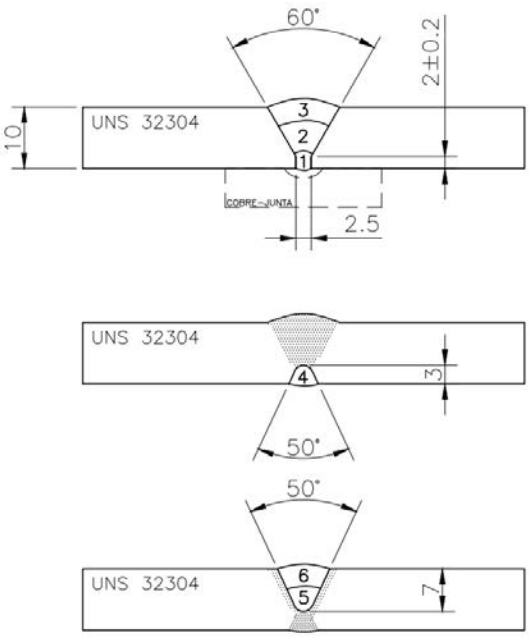

Figure 2. Dimensions of the welded specimens. Three passes in the primary welding: (1) root pass; (2) filling; (3) finishing; (4) root repair; joint repair: (5) filling; (6) finishing.

ISSN 2176-5480

3. RESULTS AND DISCUSSION

3.1 Potentiodynamic polarization curves

Potentiodynamic polarization curves of the base metal (DSS 2304), filler (DSS 2209) and repaired specimens are shown in Fig. 3. The corresponding electrochemical parameters (E_{corr}, corrosion potential; I_{corr}, corrosion current density) are presented in Tab. 3. The I_{corr} values were determined using the Tafel's extrapolation method. Results of the base metal are also shown for comparison. The results correspond to the mean value of three different specimens.

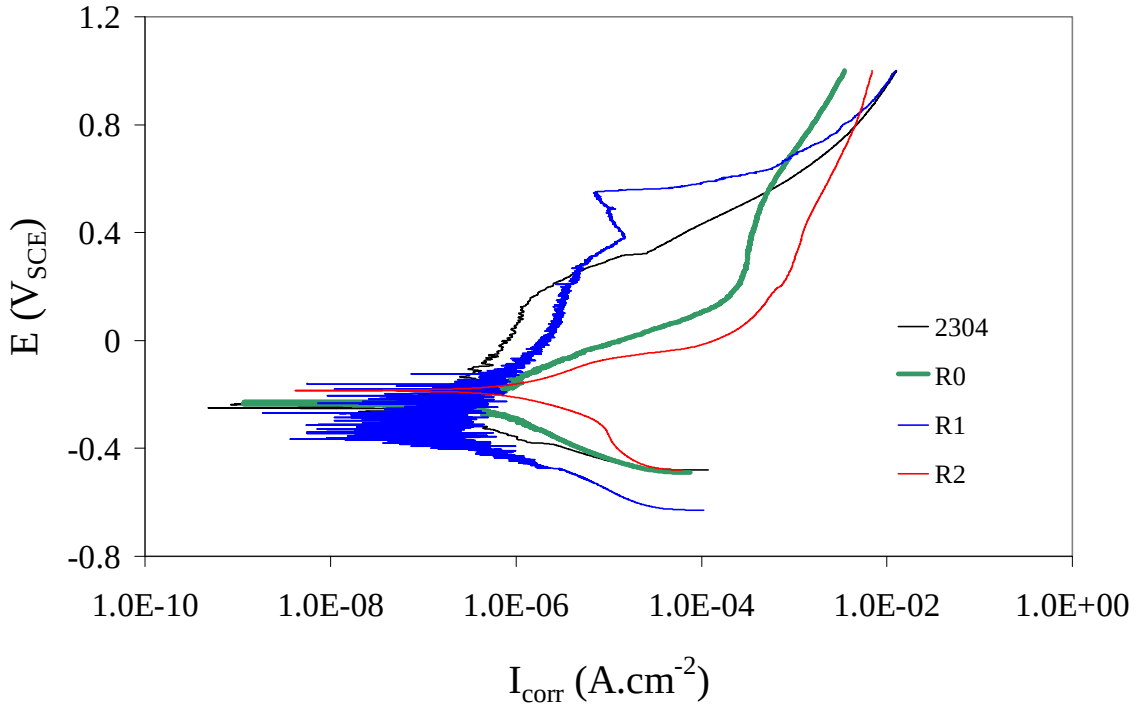

Figure 3. Potentiodynamic polarization curves of the base metal (DSS 2304), filler (DSS 2209) and repaired specimens.

Table 3. Electrochemical parameters obtained from the potentiodynamic polarization curves shown in Fig. 3.

Material	E_{corr} (mV)	I_{corr} (10^{-8} A/cm²)
2304	-235 ± 27	3.6 ± 1.2
R0	-218 ± 12	37.4 ± 26.6
R1	-327 ± 37	3.7 ± 2.0
R2	-348 ± 26	11.4 ± 7.5

The DSS 2304 base metal presented a typical passive behavior with a mean breakdown potential (E_b) of 234 ± 27 mV. The low I_{corr} values are typical materials with high corrosion resistance (Zhang et al., 2009). The homogeneous microstructure, showing a good balance between the austenite and ferrite phases, can justify this behavior. As shown in Fig. 4, the microstructure of the base metal is characterized by an approximate 1:1 proportion between austenite (brighter phase) and ferrite (darker phase) which favors the development of a high corrosion resistance DSS (Cvijovic and Radenkovic, 2006).

ISSN 2176-5480

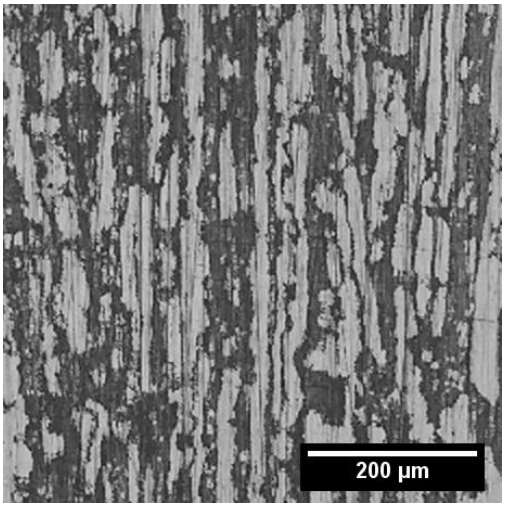

Figure 4. Optical micrograph of the 2304 steel, showing a good balance the ferrite (dark) and austenite (bright) phases.

The specimens repaired only in the root (R0) did not present a typical passive range as observed in the polarization curve shown in Fig. 3. The material is apparently active, showing a continuous increase of the current density with the applied potential. The I_{corr} is much higher than that obtained for the base metal, indicating that the R0 specimens corrode at high rate. It is known from the literature that the presence of non-metallic inclusions originated from an improper cleaning procedure after the FCAW process and deleterious chromium nitrides or carbides which precipitate during the welding operation can seriously impair the corrosion resistance of DSS (Deng et al., 2009). In this respect, the microstructure of the R0 specimen has been evaluated using SEM and optical microscopy. The SEM micrograph shown in Fig. 5 reveals the presence of a non-metallic inclusion in the weld bead of a R0 specimen.

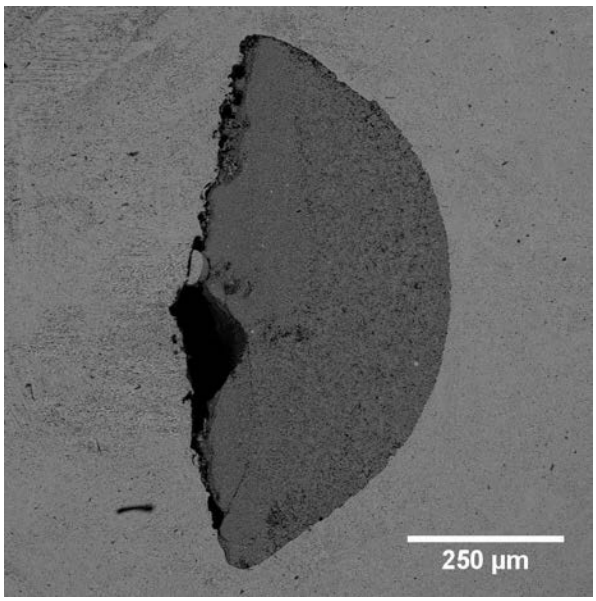

Figure 5. SEM micrograph of a non-metallic inclusion in the weld bead of a R0 specimen.

This confirms that the cleaning step after welding was not properly accomplished, suggesting that the FCAW process may not be suitable to execute repair welding cycles from the standpoint of the resulting corrosion resistance of the welded material. Moreover, the presence of such defects can also significantly reduce the mechanical strength of the weld bead (Chen et al., 2012).

ISSN 2176-5480

A complementary evaluation of the microstructure of the R0 specimens was carried out by evaluating the presence of chromium nitrides or carbides after the oxalic acid test described in section 2.3. Optical micrographs of R0 specimens are shown in Fig. 6. The presence of undesirable precipitates next to the austenite/ferrite interface was unequivocally confirmed. Even though the chemical composition of these precipitates has not been identified in the present work, Vickers microhardness measurements (Buehler, model 2100, load 50 gf) have been performed in the HAZ of the specimens whose micrographs are shown in Fig. 6. The mean hardness value was found to be 403 ± 57 HV50 which is consistent with the precipitation of deleterious carbides and nitrides after welding of DSS (Do Nascimento et al, 2008).

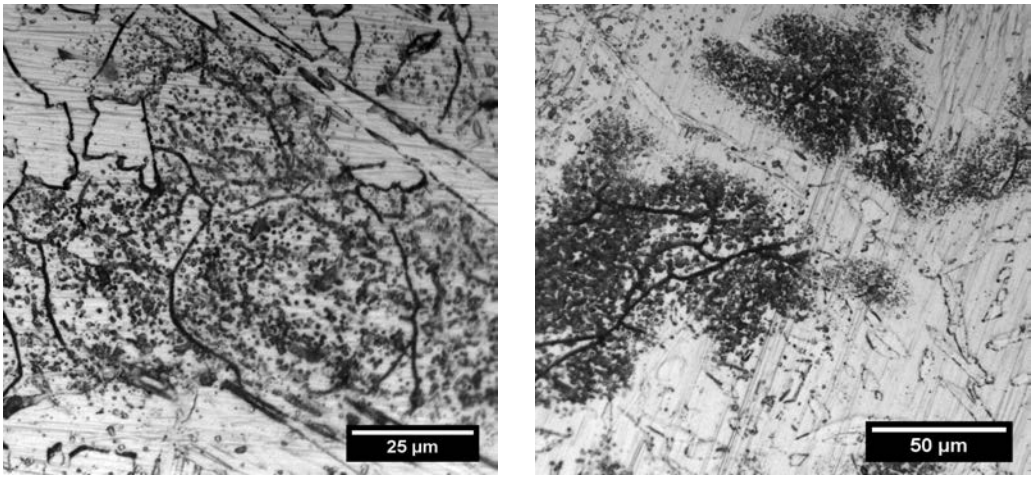

Figure 6. Optical micrographs of R0 specimens showing the presence of deleterious precipitates.

According to the results shown in Tab. 3 if one compares R1 and R2 specimens there was a trend of decreasing the corrosion potential (E_{corr}) and increasing the I_{corr} values as the number of repair cycles increased. This behavior could be explained based on the microstructural features observed in the HAZ of the specimens after each repair cycle. The corrosion current density of the R1 specimens was similar to that of the base metal. Furthermore, a well-defined passive region appears between -0.1 V and +0.53 V and a breakdown potential could be perceived at the upper limit of the passive region. For the R2 specimens the corrosion current density is higher and the polarization curve does not demonstrate any passive behavior.

In order to give a further understanding on the corrosion behavior of the R1 and R2 specimens their microstructures were observed by optical microscopy. Figure 7 presents micrographs of R1 specimens showing the base metal, fusion zone (FZ) and the interface between them in the heat affected zone. The micrograph on the right is the same region on the left but at a higher magnification to show the HAZ in more detail. The absence of deleterious precipitates is noteworthy. The high corrosion resistance of the R1 specimens should be a consequence of this favorable microstructure.

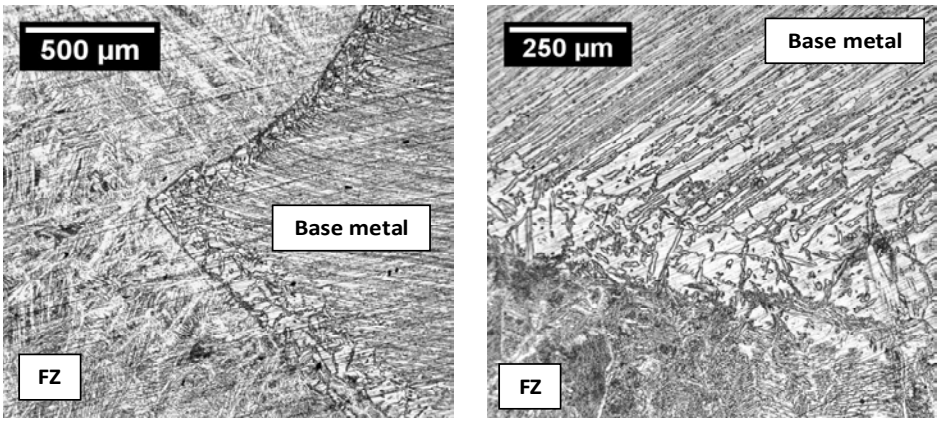

Figure 7. Micrographs of R1 specimens showing the base metal, fusion zone and heat affected zone.

ISSN 2176-5480

Optical micrographs of R2 specimens are shown in Fig. 8. The formation of deleterious precipitates can be promptly viewed. This microstructure would lead to a high corrosion current density in comparison with the R1 specimens.

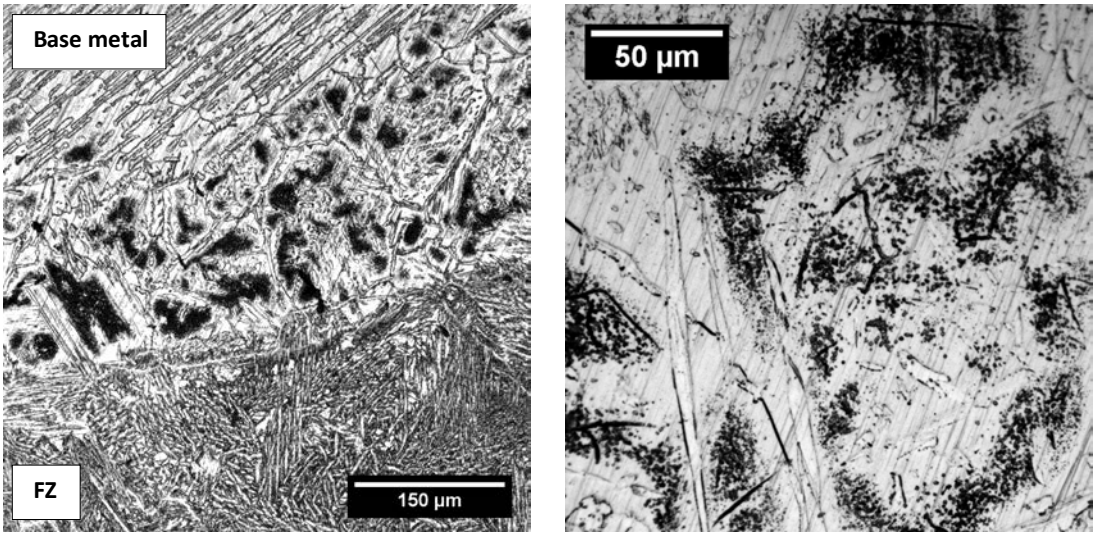

Figure 8. Optical micrograph showing the presence of precipitates in the head affect zone of an R2 specimen. The image on the right shows the head affected zone at a higher magnification.

3.2 Critical pitting temperature (CPT)

Typical curves of current density (I) versus temperature for base metal (DSS 2304) and the repaired specimens, R0, R1 and R2 are shown in Fig. 9. The criterion for determining the CPT of each specimen (temperature corresponding to a current density of 100 $A.cm^{-2}$ is marked as a horizontal line in the plot).

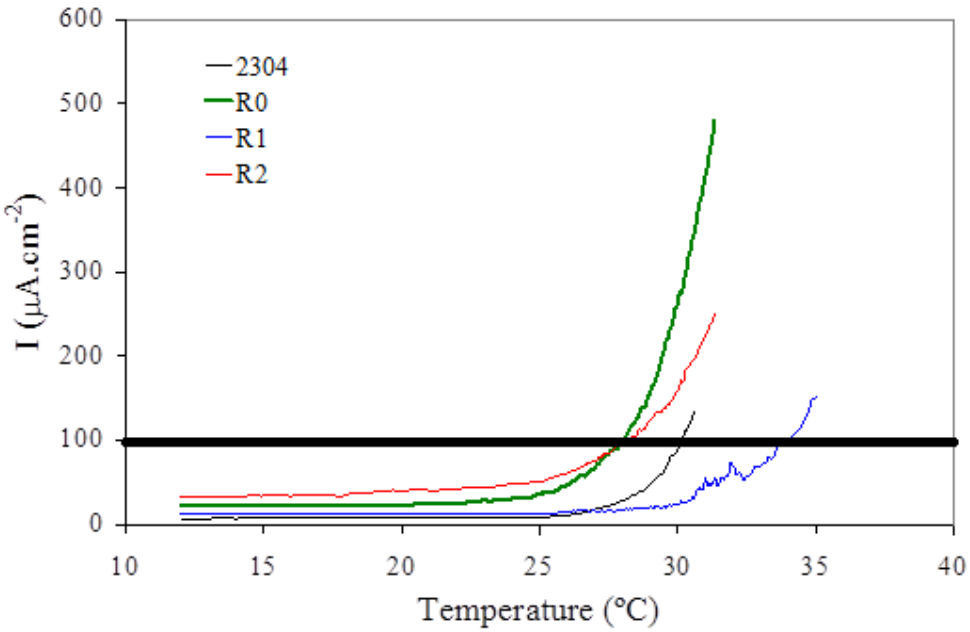

Figure 9. Typical curves of current density (I) versus temperature for base metal (DSS 2304) and the repaired specimens, R0, R1 and R2.

ISSN 2176-5480

As indicated in Fig. 9, the conditions R0 and R2 yielded the lowest CPTs (28.0 and 28.2 ºC, respectively) whereas the condition R1 presents the highest CPT (34 ºC), even higher than the value for the base metal (30.2 ºC). It is observed, thus, that R1 surpassed the pitting corrosion resistance of the specimens repaired according to the R0 and R2 conditions. This behavior can be supported by the same microstructural aspects highlighted in section 3.1. The absence of deleterious precipitates in the R1 specimens led to a high corrosion resistance and this was confirmed by the CPT values determined from the curves shown in Fig. 9. R0 and R2 specimens, in turn, presented a heterogeneous microstructure characterized by the formation of widespread undesirable precipitates in the HAZ as revealed by the oxalic acid test. Hence, the corrosion resistance was depressed for these repair welding cycles.

4. CONCLUSIONS

The influence of repair welding cycles on the corrosion behavior of the 2304 DSS has been evaluated. The results showed that it is possible to obtain a weld bead with a homogeneous microstructure after the repair cycle (R1 specimens). However, the FCAW process can lead to the presence of non-metallic inclusions in the weld bead if it is not properly cleaned after welding. The critical pitting temperature was sensitive to the microstructure transformations of the specimens during the welding process and can be used as a design criterion to assess the quality of repaired welding in DSS. A good correlation was found between the electrochemical behaviors observed in the potentiodynamic polarization curves and the CPT values.

5. REFERENCES

Charles, J. and Faria, R.A., 2008. Aços inoxidáveis duplex e aplicações em óleo e gás. ArcelorMittal. Associação Brasileira do Aço Inoxidável, p. 247.

Chen, L., Tan, H., Wang, Z., Li, J. and Jiang, Y., 2012. “Influence of cooling rate on microstructure evolution and pitting corrosion resistance in the simulated heat-affected zone of 2304 duplex stainless steels”. *Corrosion Science*, Vol. 58 (2012), p. 168.

Cvijovic, Z. and Radenkovic, G., 2006. “Microstructure and pitting corrosion resistance of annealed duplex stainless steel”. *Corrosion Science*, Vol. 48, p. 3887.

Deng, B., Wang, Z., Jiang, Y., Sun T., Xu, J. and Li J., 2009. “Effect of thermal cycles on the corrosion and mechanical properties of UNS S31803 duplex stainless steel”. *Corrosion Science*, Vol. 51, p. 2969.

Do Nascimento, A.M., Ierardi, M.C.F., Kina, A.Y. and Tavares, S.S.M., 2008. “Pitting corrosion resistance of cast duplex stainless steels in 3.5% NaCl solution”. *Materials Characterization*, Vol. 59, p. 1736.

Ogawa, T. and Koseki, T., 1989. “Effect of composition profiles on metallurgy and corrosion behavior of duplex stainless steel weld metals”. *Welding Journal*, Vol. 68, p. s181.

Tan, H., Wang, Z., Jiang, Y., Han, D., Hong, J., Chen, L., Jiang, L. and Li, J., 2011. “Annealing temperature effect on the pitting corrosion resistance of plasma arc welded joints of duplex stainless steel UNS S32304 in 1.0 M NaCl”. *Corrosion Science*, Vol. 53, p. 2191.

Tan, H., Wang, Z., Jiang, Y., Yang, Y., Deng, B., Song, H. and Li, J., 2012. “Influence of welding thermal cycles on microstructure and pitting corrosion resistance of 2304 stainless steel”. *Corrosion Science*, Vol. 55, p. 368.

Tuomi, A., Löfstrand, A. and Harju, M., 2000. “Increase usage of duplex materials in manufacturing of pulping equipment”. Duplex America Conference 2000, KCl Publishing BV, p. 401.

Zhang, L., Zhang, W., Jiang, Y., Deng, B., Sun, D. and Li, J., 2009. “Influence of annealing treatment on the corrosion resistance of lean duplex stainless steel 2101”. *Electrochimica Acta*, Vol. 54, p. 5387.

Zhang, Z., Han, D., Jiang, Y., Shi, C., Li and J., 2012. “Microstructural evolution and pitting resistance of annealed lean duplex stainless steel UNS S32304”. *Nuclear Engineering and Design*, Vol. 243, p. 56.

6. RESPONSIBILITY NOTICE

The authors are the only responsible for the printed material included in this paper.